First-principles study of hydrogenated amorphous silicon

K. Jarolimek,[1,2] R. A. de Groot,[2] G. A. de Wijs,[2] and M. Zeman[1]

[1]*DIMES, Delft University of Technology, Feldmannweg 17, 2600 GB Delft, The Netherlands*

[2]*Electronic Structure of Materials, Institute for Molecules and Materials, Faculty of Science, Radboud University Nijmegen, Heyendaalseweg 135, 6525 AJ Nijmegen, The Netherlands*

We use a molecular-dynamics simulation within density-functional theory to prepare realistic structures of hydrogenated amorphous silicon. The procedure consists of heating a crystalline structure of $Si_{64}H_8$ to 2370 K, creating a liquid and subsequently cooling it down to room temperature. The effect of the cooling rate is examined. We prepared a total of five structures which compare well to experimental data obtained by neutron-scattering experiments. Two structures do not contain any structural nor electronic defects. The other samples contain a small number of defects which are identified as dangling and floating bonds. Calculations on a bigger sample ($Si_{216}H_{27}$) show similar properties (radial distribution functions, band gap, and tail states) compared to the $Si_{64}H_8$ sample. Finally the vibrational density of states is calculated and compared to inelastic neutron-scattering measurements.

I. INTRODUCTION

Amorphous semiconductors are an important part of materials science. A lot of effort has been devoted to the research of pure amorphous silicon as a prototype of an amorphous semiconductor. Later on researchers focused on hydrogenated amorphous silicon (a-Si:H) mainly because of its technological importance. The new material brought also new challenges in understanding the peculiar role of hydrogen in the amorphous network. The main advantage of hydrogenated amorphous silicon (a-Si:H) over crystalline silicon lies in its production technique. Thin films of a-Si:H can be deposited over large areas using plasma enhanced chemical vapor deposition. The films can be deposited at low temperatures, thus allowing the use of plastic substrates. The main applications are large area electronic devices such as liquid-crystal displays and solar cells. In the visible part of the spectrum the absorption coefficient of a-Si:H is higher by an order of magnitude than that of crystalline silicon.[1] The higher absorption coefficient means less material in order to absorb the same amount of light, thus allowing for use of films less than 1 μm thick. The amorphous solar cells can be deposited on flexible substrates in a cheap roll-to-roll process.[2]

Despite the technological importance of a-Si:H many of its properties are still not yet fully understood. These include the local bonding environment of hydrogen, the structure of defects and light-induced degradation. There were several theoretical studies of a-Si:H in the past.[3–11] The accuracy of such simulations ranges from simple classical using model potentials to density functional theory (DFT). One of the first models of a-Si:H was created by Allan *et al.* using the cluster Bethe-lattice approach.[3] In 1985 Car and Parrinello (Ref. 4) were the first to use DFT to prepare a structure of pure amorphous silicon by cooling liquid silicon. Indeed most of the first-principles studies on a-Si:H follow this procedure,[5–9] while others are based on a slightly different approach. E.g., Klein *et al.*[10] prepared a sample of a-Si:H using a tight-binding molecular-dynamics simulation, by quenching a

mixture of silicon and hydrogen from the gas phase at zero pressure. Valladares *et al.*[11] proposed a cooling procedure, where they are using different time steps (not necessarily physical) to control the short-range order in the amorphous structure.

The drawback of the "cooling of the liquid" approach is the number of defects it creates. A device quality material has typically a defect concentration of 10^{17} cm^{-3}.[12] This implies that a supercell containing 10^6 atoms should have one defect. Smaller supercells should be essentially defect free, i.e., thus all silicon atoms should be four-coordinated and the sample should have a clean band gap without any defect states. This poses a severe challenge to first-principles simulations, as these are restricted by the vast computational cost to very high cooling rates. To our knowledge all previous first-principles studies on a-Si:H were hampered by this difficulty. Obtaining defect-free samples in the computer is crucial for device modeling, e.g., to determine band offsets at interfaces with a-Si:H. In this study we present structures containing low defect concentrations, generated from first-principles molecular dynamics. We demonstrate that it is in fact possible to prepare defect-free samples using the "cooling of the liquid" method. Furthermore, we investigate the convergence of the calculated properties with respect to the supercell size, showing that the band-edge features are already well described in a relatively small cell of ~72 atoms. The vibrational density of states (DOS) is calculated as another confirmation of the correct short-range order present in our samples.

This paper is organized as follows: technical details are provided in Sec. II. In Sec. III we describe the thermal procedure used to prepare amorphous structures and technical details of the calculation. In Sec. IV we discuss the effect of the cooling rate on the quality of the structures. The structural and electronic properties of samples prepared by slow cooling are discussed in Sec. V. In Sec. VI we analyze how the properties of the samples change with the supercell size. Section VII focuses on defect structures and their electronic properties. The study of the vibrational density of states is

given in Sec. VIII. Finally, conclusions are presented in Sec. IX.

II. TECHNICAL DETAILS

The total energy and forces are calculated within the DFT using a generalized gradient approximation (GGA).[13] We use the Vienna *Ab initio* Simulation Package (VASP).[14,15] Electron-ion interactions are described using the projector augmented wave method (PAW).[16,17] We use the standard PAW potentials distributed with the VASP package. The silicon potential has two reference energies for the s and p channel and one energy for the d channel. The hydrogen potential has two reference energies for the s channel and one energy for the p channel. The $1s^2 2s^2 2p^6$ electrons of silicon are kept frozen in the core. The kinetic-energy cutoff is set to 200 eV. During the whole MD run and the relaxation, we use only the Γ point for Brillouin-zone sampling. The partial occupancies are determined by the Methfessel-Paxton method (Ref. 18) with a smearing width of 0.2 eV. For calculations on the relaxed structures we use a $5 \times 5 \times 5$ Monkhorst-Pack mesh (Ref. 19) for the Brillouin Zone sampling and a Gaussian broadening of 0.05 eV.

The highest vibrational frequency which can occur during the simulation is due to the vibration of the hydrogen molecule. The silicon-hydrogen stretching mode has the second highest frequency (~ 2100 cm^{-1}).[20] The average calculated value is 2087 cm^{-1} (depending on the local environment). We set our time step to 1 fs which proves to be sufficient to describe the Si-H stretching mode. The integration of the vibrational motion of the hydrogen molecule using this time step is rather crude. However the time step of 1 fs is a reasonable compromise between computational cost and accuracy.

III. PREPARATION OF THE STRUCTURE

Hydrogen plays a vital role in saturating dangling bonds and removing electronic defect states inside the band gap. A typical device quality material for solar cell applications has a hydrogen concentration of 11 at. %.[21]

We start the preparation procedure with a periodically repeated cubic supercell containing 64 silicon and 8 hydrogen atoms. The supercell is built of 8 ($2 \times 2 \times 2$) c-Si:H cells each comprising eight silicon and one hydrogen atom. The c-Si:H cell is in fact a cubic unit cell of crystalline silicon with one hydrogen atom in the middle. The side of the supercell is set to 11.062 Å to reproduce the experimental density of 2.20 g/cm^3.

The heating and cooling of the structure was done by velocity rescaling on every MD step. The thermal procedure begins at 300 K. The velocities are initialized randomly according to a Maxwell-Boltzmann distribution. The structure is then heated to 2370 K in 1.5 ps which corresponds to a heating rate of 1.380 K/fs. At this temperature the system is a liquid. We find that the liquid sample is a metal with no trace of a gap in the density of states. This is consistent with previous calculations.[22] In order to destroy any trace of crys-
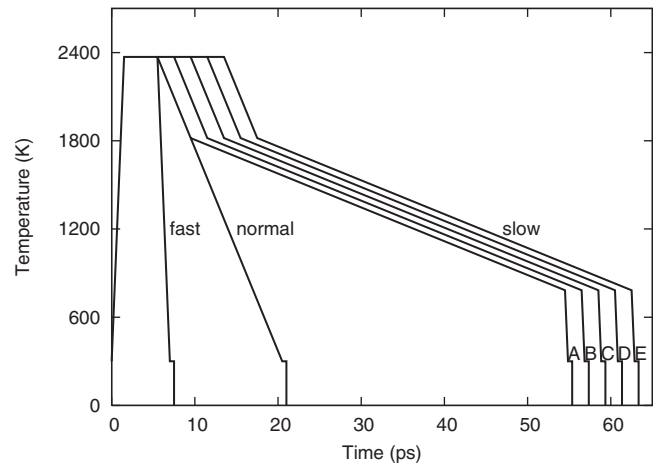

FIG. 1. The heating and cooling scheme used to prepare three samples with fast, normal and slow cooling rate. The five slow quench samples are marked with letters A, B, C, D, and E.

tallinity we let the system evolve for 4 ps. Subsequently the system is cooled back to 300 K.

We apply three different cooling procedures and study their effect (see Fig. 1). In the first and quickest procedure the cooling rate is identical to the heating rate (1.380 K/fs). We will refer to this rate as the "fast" cooling rate. In the second we cool the sample to 300 K in 15 ps resulting in a ten times slower rate (0.138 K/fs). This rate is referred to as the "normal" cooling rate. In the last cooling procedure we are actually using three different rates. From 2370 to 1818 K we follow the 0.138 K/fs rate, from 1818 to 783 K we apply the "slow" rate of 0.023 K/fs and finally from 783 to 300 K we apply again the fast rate (1.380 K/fs). The usage of three different rates is motivated by preparing a high quality amorphous structure in a short time. In the first temperature interval (corresponding to the fast cooling rate) the silicon atoms still exhibit a strong liquidlike behavior. In the second interval, being the most important, the rate used is as small as possible to allow even improbable relaxation events to occur. In the final temperature interval the atoms exhibit only vibrational movement with almost no chance of a further structural relaxation. Consequently we use the fastest cooling rate to save computer time. As can be seen in Fig. 1 we prepared a total of five different samples using the slow cooling rate. We will denote them as A, B, C, D, and E.

After reaching room temperature the system is evolved for 0.5 ps (still coupled to the thermostat) to calculate structural averages of, e.g., the radial distribution function, bond angle distribution function, and static structure factor. After calculating the structural averages the amorphous structure is quenched using the conjugated gradient method and electronic properties are calculated.

IV. EFFECT OF THE COOLING RATE

To examine the effect of the cooling rate on the quality of the amorphous structure we employ three distinct cooling procedures. We compare the different resulting samples in terms of their structure, number of defects, and electronic
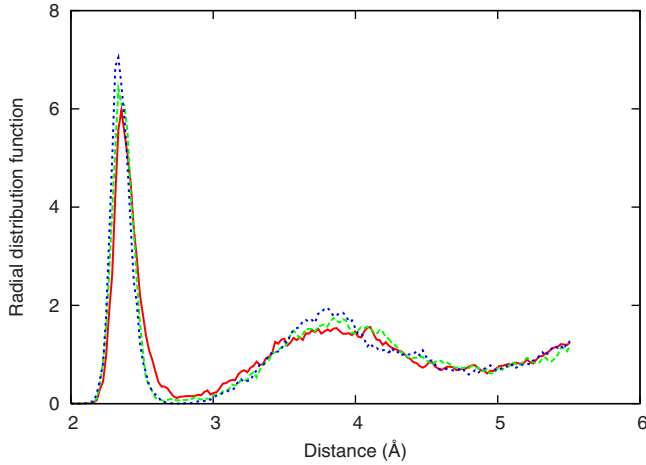
FIG. 2. (Color online) Partial radial distribution function Si-Si of three structures prepared by fast (solid red line), normal (dashed green line) and slow cooling rate (dotted blue line). The distribution function was determined for a system at 300 K.
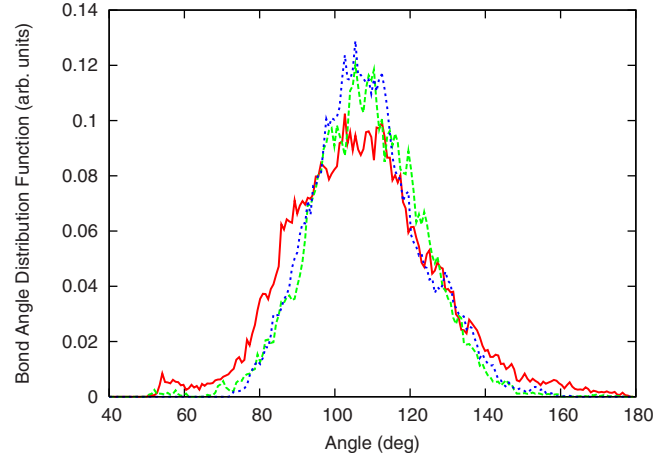

FIG. 3. (Color online) The Si-Si-Si bond angle distribution of three structures prepared by fast (solid red line), normal (dashed green line), and slow (dotted blue line) cooling rates (sample A).

properties. Thus we can assess the effect of the slower cooling rates.

A useful measure of short-range order in amorphous structures is the radial distribution function $g(r)$. It gives the probability of finding two atoms at a distance r apart. For a binary system such as a-Si:H there are three partial radial distribution functions i.e., $g_{Si-Si}(r)$, $g_{Si-H}(r)$, and $g_{H-H}(r)$. We show the silicon-silicon radial distribution function after the different cooling rates in Fig. 2. We observe that slower cooling results in better-defined peaks with higher values of the first and second maximum of $g_{Si-Si}(r)$. With slower cooling rates the value of the first minimum in $g_{Si-Si}(r)$ is decreasing toward zero.

To define other correlation functions we need to determine a cutoff distance for the silicon-silicon and the silicon-hydrogen bond. If a distance between two atoms is smaller than the cutoff distance, they are considered to be bonded. The cutoff distance of the silicon-silicon bond was set to 2.76 Å corresponding to the position of the first minimum in $g_{Si-Si}(r)$. Similarly the cutoff distance of the silicon-hydrogen bond was set to 1.79 Å matching the position of the first minimum in $g_{Si-H}(r)$. The cooling rate does not change the position of the first minimum in $g_{Si-Si}(r)$ and $g_{Si-H}(r)$, which justifies the usage of the same cutoff distances for all the prepared samples.

The average Si–Si coordination number N_c for the normal and slow cooling rates approaches the expected value for

a-Si:H with 11 at. % of hydrogen (see Table I). If we suppose that a-Si:H has a total coordination number of 4, i.e., the material is defect free and that the hydrogen atoms are used solely to saturate dangling bonds. Then we should have a coordination number of 3.89 for a material containing 11 at. % hydrogen. The mean first-neighbor distance r_1 decreases with slower cooling and approaches the experimental values (see Table III). A decreasing trend is also observed for the second-neighbor distance r_2. The parameters related to the second-neighbor peak are calculated from distances between two silicon atoms bonded to a common atom. The mean values are calculated as averages over 500 MD steps with the samples at 300 K. The deviations of the first- and second-neighbor distances are due to static disorder and were calculated at 0 K. The experimental values of σ_1 and σ_2 are usually obtained by peak fitting of the Si-Si radial distribution. The experimental distributions are broadened by thermal vibration and by real-space resolution. To calculate the static deviations it is then necessary to subtract the thermal and experimental broadening of a c-Si sample. Note, that although this method is often used, it is an approximation.

Further, we calculate the bond angle distribution function, which gives the distribution of angles between two silicon-silicon bonds connected to a common silicon atom (see Fig. 3). The bond angle distributions of samples obtained via the slow cooling rate are essentially identical (In Fig. 3 we depict only that of sample A). The peak centered around the tetrahedral bond angle ($\sim109.5°$) narrows with slower cool-

TABLE I. Structural properties of samples prepared by fast, normal, and slow cooling rates: coordination number N_c, mean first-neighbor distance r_1, deviation of the first-neighbor distance σ_1, mean second-neighbor distance r_2, deviation of the second-neighbor distance σ_2, mean bond angle θ, and deviation of the bond angle σ_θ. The mean values and the coordination number are calculated at 300 K, the deviations refer to static disorder and are calculated at 0 K. The values of the slow rate are averaged over the five samples.

Structure	N_c	r_1	σ_1	r_2	σ_2	θ	σ_θ
Fast	3.97	2.417	0.058	3.855	0.401	107.731	16.55
Normal	3.86	2.386	0.061	3.852	0.353	108.891	14.25
Slow (average)	3.89	2.377	0.049	3.840	0.326	108.894	13.57

TABLE II. Types of neighboring environments for three structures prepared by fast, normal, and slow cooling rates. The expression Si_3H_1 denotes that the given atom has a total number of four neighbors, three of which are silicon atoms and one is a hydrogen atom.

Structure	Si_2H_2	Si_3H_0	Si_3H_1	Si_4H_0	Si_4H_1	Si_5H_0
Fast	1	0	6	55	0	2
Normal	0	3	7	53	1	0
Slow (sample A)	1	0	4	59	0	0

ing rate. The bond angle deviation σ_θ changes from 16.55° to 13.57° for fast and slow cooling rates, respectively. Again these values are due to static disorder and were calculated at 0 K. Note that the sample prepared by the fast cooling rate has also a peak at 55°. This is a residue of the metallic bonding in the liquid. As was shown by Štich *et al.*[22] this peak can reach the same intensity as the tetrahedral one in liquid silicon.

The healing power of slow cooling is even more visible in the electronic properties. The number of structural defects responsible for the in-gap states decreases with slower cooling (see Table II). This trend can be also followed in the calculated density of states; see Fig. 4. Here the DOS of the different samples are aligned for clarity. The zero of the energy scale is chosen to coincide with the average of the Kohn-Sham eigenvalues of all the occupied states. Note that the slow quench structure has neither structural defects nor electronic defect states in the gap. The tendency of improving the quality of the structure with slower cooling is exactly what one would intuitively expect. What is not so obvious is whether the rate of the order of 0.01 K/fs is sufficient. The correlation functions of the slow quench sample however
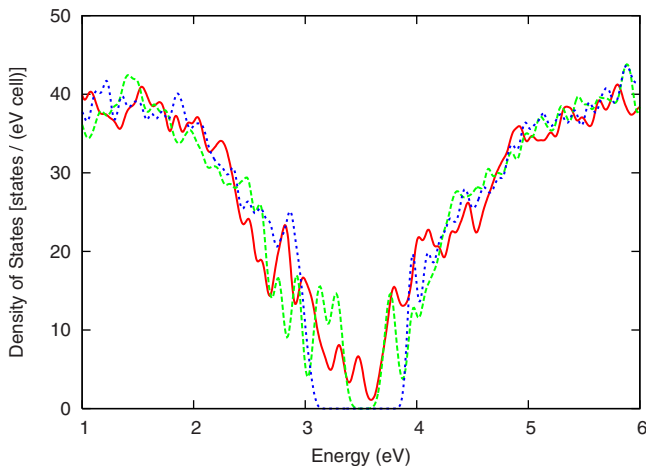

FIG. 4. (Color online) Density of states of three structures prepared by fast (solid red line), normal (dashed green line), and slow (dotted blue line) cooling rates (sample A). The DOS functions are aligned for clarity. The positions of the Fermi levels are: 3.61, 3.52, and 3.27 eV for the fast, normal, and slow cooling rate, respectively.
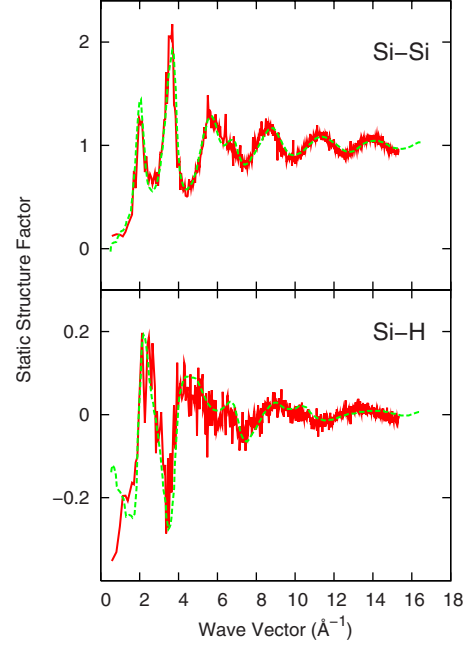

FIG. 5. (Color online) Partial static structure factors averaged over five slow quench samples (red solid line) and compared to neutron-scattering measurements (green dashed line) (Ref. 28). All structure factors use the Ashcroft and Langreth formalism. Both curves refer to systems at 300 K.

reproduce the experimental ones and the sample is essentially defect free. This suggests that the slow cooling rate is indeed sufficient to prepare realistic amorphous structures.

V. STRUCTURES OBTAINED BY SLOW COOLING

All five structures prepared by slow cooling (A, B, C, D, and E) start from different liquid configurations separated in time by 2 ps at the temperature 2370 K (see Fig. 1). The radial distribution functions as well as the static structure factors are averaged over the five slowly quenched samples and compared with neutron-diffraction measurements.[28]

The static structure factor is a quantity proportional to the diffracted intensity in an x-ray or neutron-diffraction experiment. For a binary compound there are three partial static structure factors. We calculate them according to the definition of Ashcroft and Langreth,[29]

$$S_{ij}(q) = \frac{1}{\sqrt{N_i N_j}} \left[\left\langle \sum_\mu^{N_i} \sum_\nu^{N_j} e^{-i\boldsymbol{q} \cdot (\boldsymbol{R}_{i\mu} - \boldsymbol{R}_{j\nu})} \right\rangle - \delta_{\boldsymbol{q},0} \right], \quad (1)$$

where N_i and N_j denote the number of atoms of species i and j, respectively, $\boldsymbol{R}$ are the position vectors of the atoms and $\boldsymbol{q}$ is a vector in reciprocal space. The averaging is performed over different $\boldsymbol{q}$ which have the same length (we consider only vectors $\boldsymbol{q}$ on the reciprocal lattice). The resulting structure factor is then averaged over different configurations during a 0.5 ps time interval at the temperature of 300 K. As seen in Fig. 5 the agreement between theoretical and experimental silicon-silicon structure factor (Ref. 28) is good. We are able to reproduce the first two peaks as well as the fol-

lowing peaks up to 15 Å^{-1}. The agreement is worse for the other partial static structure factors. This is due to the very small number of hydrogen atoms, resulting in a poor statistics. Another source of discrepancy is that we treat the hydrogen atom as a classical particle. Note that Bellisent *et al.* use a material with 16 at. % of hydrogen.

The radial distribution $g_{\alpha\beta}(r)$ for a binary compound is defined as the number of particle pairs $N^{sys}(r)$ in the system, relative to the number of pairs we would find in an ideal gas. The number of β atoms that are at the distance r apart from atoms of type α is

$$N^{sys}(r) = \sum_{I=1}^{N_\alpha} \sum_{J=1}^{N_\beta} \delta(r - |\mathbf{R}_I - \mathbf{R}_J|), \qquad (2)$$

where $\mathbf{R}$ are the position vectors of atoms and N is the number of atoms of a particular species. For atoms that are randomly distributed is space, we get

$$N^{gas}(r) = N_\alpha \left(4\pi r^2 \frac{N_\beta}{V} \right), \qquad (3)$$

where V is the volume of the system. Thus the theoretical radial distributions $g_{\alpha\beta}(r)$ are calculated according to the expression,

$$g_{\alpha\beta}(r) = \frac{V}{4\pi r^2 N_\alpha N_\beta} \sum_{I=1}^{N_\alpha} \sum_{J=1}^{N_\beta} \delta(r - |\mathbf{R}_I - \mathbf{R}_J|). \qquad (4)$$

The experimental radial distributions are obtained by Fourier transforming the static structure factor.[30] Comparing the calculated and measured radial distributions in Fig. 6 we find very good agreement in the peak positions. However, there is a major difference in the intensity of the first peak, in both, the Si-Si and Si-H partials. This discrepancy is mainly due to two reasons. First the peak height depends on the experimental resolution. We studied several experimental Si-Si radial distribution as measured by Bellisent *et al.*,[28] Fortner *et al.*,[31] Kugler *et al.*,[32] and Laaziri *et al.*[23] We observe that increasing the maximum momentum value Q_{max} from 16 up to 55 Å^{-1} considerably sharpens the peak and increases its height. The samples in these measurements were not identical, but sufficiently similar to warrant this comparison.

The second source of discrepancy is the neglect of the quantum nature of the nuclei. So far we have treated the atomic nuclei as classical particles, thus overestimating the peak heights. Here we follow the method outlined by Giacomazzi *et al.*[33] to account for the quantum effects. The delta function in Eq. (4) is replaced by a Gaussian function normalized to one and with a variance of

$$\sigma_{IJ}^2 = \langle [\mathbf{d} \cdot (\mathbf{u}_I - \mathbf{u}_J)]^2 \rangle, \qquad (5)$$

where $\mathbf{d}$ is a unit vector pointing in the direction of $\mathbf{R}_J - \mathbf{R}_I$. $\mathbf{R}_I$ and $\mathbf{R}_I$ denote equilibrium positions of the Ith and Jth atoms, respectively. $\mathbf{u}_I$ is the displacement of the Ith atom with respect to $\mathbf{R}_I$. The brackets $\langle \cdots \rangle$ symbolize a thermal average. The various contributions are obtained as follows:
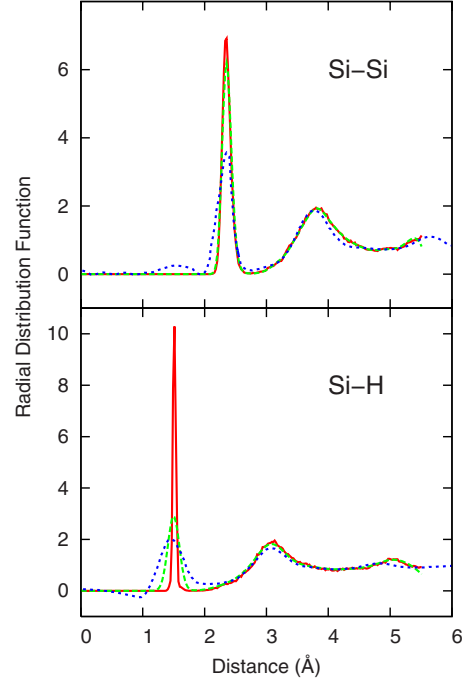

FIG. 6. (Color online) Partial radial distributions averaged over 500 MD configurations (red solid line), calculated radial distributions with quantum corrections (dashed green line), and neutron-scattering measurements (blue dotted line) (Ref. 28). Both types of calculated curves are averages over five slow quench samples. All curves refer to systems at 300 K.

$$\langle u_{Ii} u_{Jj} \rangle = \sum_n \frac{\hbar}{\omega_n} \frac{\xi_{Ii}^n}{\sqrt{M_I}} \frac{\xi_{Jj}^n}{\sqrt{M_J}} \left[n_B(\hbar\omega_n) + \frac{1}{2} \right], \qquad (6)$$

where the i and j subscripts denote Cartesian components. The sum runs over vibrational modes n with eigenmodes ξ^n and eigenfrequencies ω_n. The vibrational modes are calculated via the finite differences method available in the VASP package (see, e.g., Kresse *et al.*[34]). M_I is the mass of the Ith atom. The Boson occupation number n_B is calculated according to

$$n_B(\hbar\omega) = \frac{1}{e^{\hbar\omega/k_B T} - 1}, \qquad (7)$$

where k_B is the Boltzmann constant and T is the temperature of the system.

The calculated radial distributions that take quantum effects into account are depicted in Fig. 6. The Si-Si partial distribution remains unchanged due to the relatively high mass of silicon atoms.[35] We do, however, see a considerable change in the Si-H distribution, where the height of the first peak decreases to a third of the original one. Thus after applying the quantum corrections we get much better agreement with experiment. However, the calculated peaks are still above the measured ones, due to lack of experimental resolution.

Parameters such as the coordination number (area under the first peak) and average bond length are less affected by experimental resolution. It is thus more meaningful to com-

TABLE III. Properties of the five samples prepared by slow cooling rate: coordination number N_c, mean first-neighbor distance r_1, deviation of the first-neighbor distance σ_1, mean second-neighbor distance r_2, deviation of the second-neighbor distance σ_2, mean bond angle θ, deviation of the bond angle σ_θ compared to experimental values. The mean values and the coordination number are calculated at 300 K, the deviations refer to static disorder and are calculated at 0 K. The percentages in the first column denote hydrogen concentrations. The last column lists calculated band-gap values.

Structure	N_c	r_1	σ_1	r_2	σ_2	θ	σ_θ	band gap (eV)
A	3.91	2.373	0.048	3.835	0.329	108.98	13.74	0.86
B	3.87	2.376	0.049	3.850	0.283	108.99	11.42	1.06
C	3.88	2.361	0.040	3.813	0.315	108.87	13.27	0.91
D	3.92	2.383	0.044	3.835	0.367	108.63	15.46	0.79
E	3.86	2.391	0.057	3.867	0.326	109.01	13.59	0.98
Average	3.89	2.377	0.049	3.840	0.326	108.89	13.57	0.92
Laaziri[a] *a*-Si	3.88 ± 0.01	2.351 ± 0.001	0.031 ± 0.001	3.80 ± 0.01	0.23	107.83 ± 0.97	9.63 ± 0.08	
Filipponi[b] *a*-Si:H, 8%	3.88 ± 0.12	2.35 ± 0.01						
Vignoli[c] *a*-Si:H, 12%	3.71 ± 0.07	2.37 ± 0.04					8.7	
Wakagi[d] *a*-Si:H, 12.8%	4.0	2.363 ± 0.004	0.038 ± 0.008				9.3	
Schülke[e] *a*-Si:H, 33%	3.4 ± 0.1	2.363 ± 0.008		3.86 ± 0.01	0.187 ± 0.005	109.5 ± 1.0	7.9 ± 0.4	

[a]Reference 23.
[b]Reference 24.
[c]Reference 25.
[d]Reference 26.
[e]Reference 27.

pare the coordination number and average bond length than the peak intensities (for the first peak). Unfortunately Bellisent *et al.* did not publish coordination number values for their measurement. We summarize several calculated and experimental structural parameters for the Si-Si partial distribution in Table III.

The average Si-Si coordination number coincides with the expected value for a defect-free material containing 11 at. % of hydrogen. We note that the experimental values differ significantly. Laaziri *et al.* showed that scattering data out to at least 40 Å^{-1} are necessary to reliably determine the value of N_c. The relative differences between the measured values of r_1 are approximately 1%. The same holds for differences between our results and the experiment. The calculation overestimates the static deviation of the first-neighbor distance σ_1. The comparison to experimental values indicates that the model contains more static disorder, although some of the slow quench samples fall into the uncertainty range of σ_2 reported by Wakagi *et al.* The calculated average second-neighbor distance r_2 coincides with neutron-scattering measurements (Refs. 28 and 36) and with the crystalline silicon value. The value reported by Laaziri *et al.* is lower than the other experimental values. Laaziri *et al.* note that this can be due to contributions from the third peak in the Si-Si radial distribution that affect the peak fitting parameters. Consequently the bond angle reported by Laaziri *et al.* is lower than values reported by Schülke *et al.* and Bellisent *et al.*,[28] and is lower than the tetrahedral angle in c-Si (109.47°). The bond angle deviation σ_θ measured by Schülke is the lowest value compared to measurements of Wakagi *et al.* and Vignoli *et al.* This can probably be attributed to the large amounts of hydrogen (33 at. %) present in the sample. Vignoli *et al.* and Wakagi *et al.* obtain the bond angle deviation

in an indirect way using the Raman spectra. They use a model, where the angle deviation depends linearly on the width of the TO peak. Vignoli *et al.* measured a deviation of 8.7° for an a-Si:H sample containing 12 at. % of hydrogen. Laaziri *et al.* obtain the bond angle deviation from the width of the second peak in the silicon radial distribution. They subtract the thermal disorder and experimental resolution utilizing the values measured on c-Si samples. Laaziri *et al.* report that the angle deviation value of 9.63° agrees well with previous studies. However they point out that the result has to be treated with caution, since the second peak can contain contributions from the third peak and this can affect the fitting parameters. We note that our average value of the bond angle deviation is lower compared to previous calculations of Gupte *et al.* (21.7°) (Ref. 8) and Klein *et al.* (16.6°).[10] The trend that theoretical calculations (including our calculation) overestimate the bond angle deviation is rather clear. The same trend is observed in the deviation of the second-neighbor distance since these two parameters are closely connected. We would like to point out that the angle deviation is a very sensitive parameter. The five slow quench samples exhibit a significant variation in the angle deviation. On the contrary other parameters are very similar.

The experimental information available on the Si-H partial distribution is more sparse than on the Si-Si one. The calculated position of the first peak is found to be 1.51 Å. We note that the calculated value of 1.51 Å is identical to the calculated silicon-hydrogen bond length in the silane molecule. The calculated hydrogen-hydrogen radial distribution (not shown) has a peak at 0.75 Å, corresponding to the hydrogen molecule bond. Hydrogen molecules are found in samples A and D. The statistics in the hydrogen-hydrogen radial distribution function is very poor, rendering any comparison with the experiment unreliable.
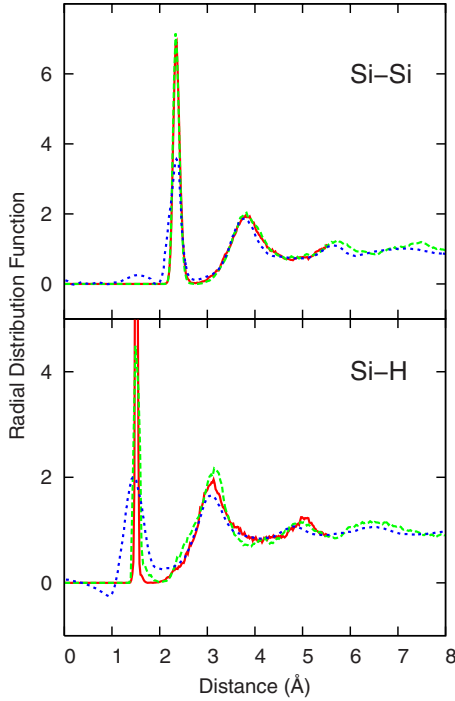
FIG. 7. (Color online) Partial radial distribution functions of the small supercell (red solid line), big supercell (green dashed line) compared to neutron-scattering measurements (blue dotted line) (Ref. 28). All curves refer to systems at 300 K.

The band-gap values for all slow quench samples are summarized in Table III. The reported band gaps are calculated as a difference between the energy of the lowest unoccupied state and the highest occupied state, *leaving out the defect states*. Defect states are identified on the basis of their localized nature. The average band gap is found to be 0.92 eV with a standard deviation of 0.10 eV. The experimental value for a device quality material is 1.7 eV,[37] almost two times higher than the theoretical value. However, this discrepancy is not surprising at the level of the DFT approximation. In the case of crystalline silicon the situation is similar: the calculated band gap is 0.61 eV and the experimental value is 1.17 eV.[38] Note that in both the theoretical and experimental case the band gap of a-Si:H is larger than that of c-Si.

VI. CONVERGENCE IN THE SUPERCELL SIZE

To study the effect of the supercell size on the calculated properties we performed a calculation on a bigger supercell containing 216 silicon and 27 hydrogen atoms. The preparation procedure is analogous to the preparation of smaller supercells by slow cooling, employing the same rates. The initial supercell is now build of 27 ($3 \times 3 \times 3$) c-Si:H cells. The silicon-silicon radial distribution of the small and big cell closely resemble each other (see Fig. 7). They both reproduce the experimental curve up to a distance of 5.5 Å, with correct positions of the first and second peak. The calculated position of the third peak (only visible in the big cell) is a bit higher than the experimental value. The positions of the first

and second peak in the silicon-hydrogen radial distribution are 1.51 and 3.15 Å, respectively, in both the small and big sample. The coordination number of the big sample is 3.87, a value close to the averaged value of the small samples (3.89). The mean first-neighbor distance is 2.374 Å with a static deviation of 0.041 Å. The mean second-neighbor distance is found to be 3.838 Å with a static deviation of 0.302 Å. Thus we find that the mean values of the first- and second-neighbor distance do not change significantly if one uses bigger supercells. The static deviations of the big supercell are found to be lower than the average deviations of the small supercells. It is however difficult to draw any conclusions from that, since the deviation values vary considerably among the small samples. Note that for example sample C has a lower σ_1 value than the big sample and sample B has a lower σ_2 value than the big sample. The average bond angle of the big sample (108.89°) is identical to the averaged value of the small samples. By analogy to σ_2, the bond angle deviation of the big sample is lower than the average of the small samples. The value of σ_θ due to static disorder is 12.54°. The band gap of the big sample is found to be 0.90 eV, a value close to the average band gap of the smaller samples.

Due to the structural disorder present in amorphous semiconductors, band tails are formed in the vicinity of the valence- and conduction-band edges. In order to better characterize the band tails, we employ the so-called participation ratio p_i, which is a measure of localization of the eigenstates ψ_i. It is calculated by projecting the wave function ψ_i onto spherical harmonics, which are nonzero only in spheres centered on each atom j. The participation ratio is defined as follows (see, e.g., Ref. 39):

$$p_i = \left(\sum_{j=1}^{N} \sum_{l=1}^{3} c_l^2(\boldsymbol{R}_j) \right)^2 \left(N \sum_{j=1}^{N} \sum_{l=1}^{3} c_l^4(\boldsymbol{R}_j) \right)^{-1}. \qquad (8)$$

The sums run over angular-momentum components l and over each atom with coordinates $\boldsymbol{R}_j$. The order of the spherical harmonics function m is already absorbed in the expansion coefficients c_l. According to this definition $p_i \sim 1$ for a delocalized state (e.g., plane wave) and approaches the value N^{-1} for a localized state, where N is the number of atoms. In Fig. 8 we show the participation ratio of every electronic state in our big supercell. We note that some of the states ψ_i have a participation ratio higher than 1. This error arises from the projections inside the spheres centered on the atoms. The spheres can partially overlap but still do not fill the whole volume of the supercell.

Figure 8 clearly shows the different regimes of localization typical of an amorphous semiconductor: the valence-band region (from −10 to −1 eV), valence-band tail region (from −1 to −0.6 eV), band-gap region (from −0.6 to 0.3 eV) with very localized defect states, conduction-band tail region (from 0.3 to 1 eV) and the conduction-band region (from 1 eV) with delocalized states. The existence of band tails was predicted in the early model of amorphous semiconductors by Anderson.[40] It is well established experimentally by measurements of electrical transport, doping, and recombination.[12] In fact the electronic properties of the
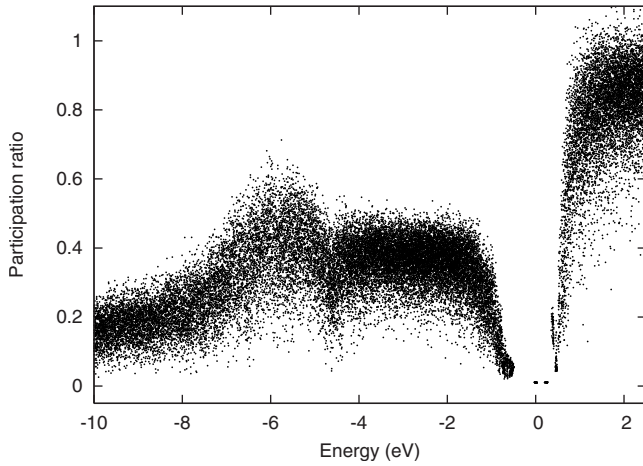
FIG. 8. Participation ratio vs energy of the $Si_{216}H_{27}$ supercell. Each dot represents a distinct Kohn-Sham state. The Brillouin-zone sampling was done with a $5 \times 5 \times 5$ Monkhorst-Pack mesh.

amorphous semiconductors, which differ considerably from their crystalline counterparts, are due to the band tails.

VII. STRUCTURAL AND ELECTRONIC DEFECTS

Although creating structures without any defects is important, on the other hand a small number of defects can give valuable information about the structure and electronic properties of defects in a-Si:H. Three out of five samples (B, D, and E) contain one dangling bond (undercoordinated atom) and one floating bond (overcoordinated atom) each. The big supercell contains one dangling bond and two hydrogens in a bond-centered (BC) position. Two samples, namely A and C, have no structural defects (see Table IV). The calculated densities of states of these defect-free samples are shown in Fig. 9.

Even though there is no one-to-one correspondence between a structural defect and an electronic defect state (as pointed out by Drabold *et al.*[41]), we were able to assign almost all electronic defects to defect atoms.[42] In Fig. 10 we show the calculated density of states for the samples containing defect states inside the gap. The defect state B1 is a dangling bond with the charge density localized on a three-

TABLE IV. Types of local environments of structures prepared by slow cooling. The expression Si_3H_1 denotes that the given silicon atom has a total number of four neighbors, three of which are silicon atoms and one is a hydrogen atom. The last column gives the number of H_2 molecules in the sample.

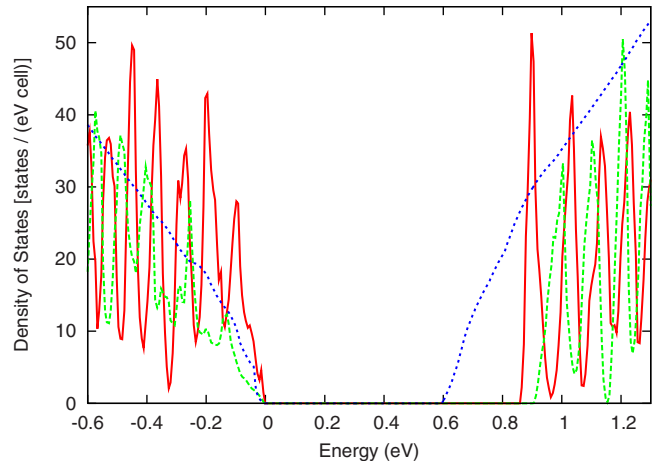| Structure	Si_2H_2	Si_3H_0	Si_3H_1	Si_4H_0	Si_5H_0	H_2
A	1	0	4	59	0	1
B	0	1	8	54	1	0
C	1	0	6	57	0	0
D	2	1	2	58	1	1
E	1	1	6	55	1	0
F (big cell)	0	1	27	188	0	1

FIG. 9. (Color online) Calculated density of states of the slow quench samples: sample A (red solid line), sample C (green dashed line), and c-Si (blue dotted line). The values for c-Si were multiplied by a factor of 100. The zero of energy was chosen at the top of the valence-band edge.

fold coordinated atom. The defect state B2 is a floating bond with the charge density centered around a fivefold coordinated atom. In this case the charge density is pushed toward the neighboring atoms, contrary to the dangling-bond defects, where it is localized on the defect atom itself. This finding is consistent with previous calculations.[43] The situation is very similar in the case of sample D. The D1 state is a dangling bond with charge density localized on a threefold coordinated atom. The D2 state is a floating bond with the charge density localized around a fivefold coordinated atom. The interpretation becomes more difficult in sample E. For the E1 state it is difficult to decide whether it is a dangling or a floating bond. In this case the defect structures share atoms
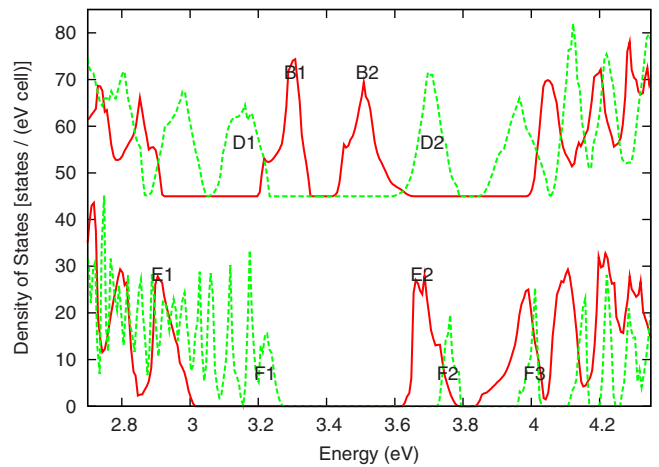

FIG. 10. (Color online) Calculated density of states of the slow quench samples containing in-gap states: sample B (solid red line), sample D (dashed green line), sample E (solid red line), and sample F (dashed green line). The sample F is the big cell. The density of states of the samples B and D are shifted for clarity. The DOS functions are aligned for clarity. The Fermi levels are positioned at: 3.39, 3.42, 3.22, and 3.75 eV for the samples B, D, E, and F, respectively.
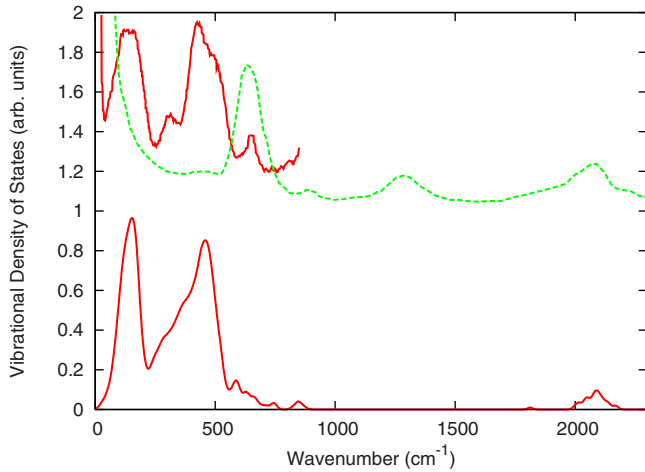
FIG. 11. (Color online) Upper figure: inelastic neutron-scattering experiments on a-Si:D (solid red line) and on a-Si:H (dashed green line). Lower figure: calculated vibrational density of states averaged over five slow cooling samples (solid red line).

and the charge density of the E1 state is contributing to both of them. The state E2 is a dangling bond with the charge density centered on the undercoordinated atom. Sample F (the big cell) contains three defect states. The F1 state is a dangling bond, the states F2 and F3 are due to BC hydrogen. The BC hydrogen defect was proposed by Fish and Licciardello[44] and was found also in previous MD simulations.[8] The average Si–H bond length is found to be 1.71 Å and the average Si-H-Si angle is 148.4°. The charge density of the interstitial hydrogen defect is distributed equally between the two Si-H bonds and is localized closer to the silicon atoms.

VIII. VIBRATIONAL DENSITY OF STATES

The vibrational density of states was calculated for each of the five samples resulting from slow cooling. We used the finite differences method (see, e.g., Kresse $et\ al.$[34]) in which all the atoms were displaced by 0.01 Å in the direction of each Cartesian coordinate, both positive and negative. For each displacement forces are calculated as a derivative of the total energy and the dynamical matrix is obtained. The diagonalization provides us with eigenfrequencies of the particular modes. These were broadened with Gaussians with a width of 0.1 eV.

Experimentally the vibrational density of states can be obtained from inelastic neutron-scattering measurements. The situation is complicated by the large neutron-scattering cross section of hydrogen compared to that of silicon. As a result the spectrum of a-Si:H is dominated by the hydrogen vibrations. To overcome this problem Sinclair and co-workers performed also measurements on deuterated samples, replacing the 22% of hydrogen by deuterium.

In Fig. 11 we compare our calculated vibrational DOS with the experimental DOS by Sinclair $et\ al.$[45] The region from 0 to 550 cm^{-1} is due to vibration of the silicon network. There are two prominent peaks at 150 and 460 cm^{-1}. These are the transverse acoustic and transverse optical

modes, which are also present in crystalline silicon. There were several studies on pure a-Si (Refs. 4, 22, and 46–50) giving essentially the same results, although they can differ in the exact peak positions. Note that the peak at 460 cm^{-1} is highly asymmetric. This is probably because it is a superposition of the transverse optical mode and the longitudal modes.

The region from 530 to 750 cm^{-1} is due to SiH wagging, SiH_2 wagging and SiH_2 twisting modes. The frequency regions of the particular modes overlap and depend on the local environment. The experimental peak due to this group of modes is located at 640 cm^{-1} and is much more noticeable. The peak at 850 cm^{-1} is arising from a SiH_2 bending (scissors) mode and is also clearly visible in the experimental spectrum. Sinclair $et\ al.$ resolved the peak in the hydrogenated sample at 1280 cm^{-1} as a second overtone of the SiH_n rocking and wagging mode. The SiH stretching modes have frequencies from 1810 to 2170 cm^{-1}. The stretching frequencies of the SiH_2 group have higher frequencies from 2070 to 2140 cm^{-1}. The large spread of frequencies in the stretching modes is also visible in the experiment. The mode with the highest frequency is the H_2 stretching mode from 4150 to 4190 cm^{-1}.

As mentioned above the big supercell contains two hydrogen atoms in a BC position. This should give rise to unique modes in the vibrational density of states. We calculated their frequencies in the big cell allowing the two hydrogens, the four silicon atoms making up the bridges and their nearest neighbors to move. This should be a reasonable approximation since a hydrogen atom is ∼28 times lighter than a silicon atom. The Si_2H wagging mode has a frequencies from 620 to 670 cm^{-1}, the Si_2H bending mode has frequencies from 750 to 800 cm^{-1}. These modes overlap with the SiH_n wagging and bending modes, thus will be difficult to observe. However the Si_2H stretching frequencies are 1050 and 1410 cm^{-1} and are clearly separated from all the SiH_n modes.

IX. CONCLUSIONS

First-principles molecular-dynamics simulations of a-Si:H were carried out. We examined the effect of the cooling rate on the quality of the amorphous structure. A substantial improvement of structural and electronic properties was found with slower cooling. The slow cooling rate and the size of the $Si_{64}H_8$ supercell seem to be sufficient to prepare realistic amorphous structures, with low defect concentrations. Further, we obtained good agreement with the experimental static structure factor and radial distribution functions from neutron-scattering measurements. Other structural properties such as the coordination number N_c, mean nearest-neighbor distance $\bar{r}$, rms deviation of the bond length σ_r differ by no more than 1% compared to values measured by extended x-ray-absorption fine structure (EXAFS). The average DFT band gap is found to be 0.92 eV, a value higher than the DFT band gap in crystalline silicon. Interestingly, the simulations reveal that the presence of hydrogen molecules in a-Si:H is possible. The calculations performed on a big supercell give similar structural and electronic properties of the amorphous

network, facilitating the use of smaller supercells. Participation ratio as a function of energy demonstrates the localized nature of band tail states. Two out of five slow quench samples contain neither structural defects nor electronic defect states in the gap. In the other the samples we find dangling and floating bond defects and couple them to undercoordinated and overcoordinated atoms, respectively. The big cell sample contains hydrogen in a bridging position, giving states in the gap. The calculated vibrational density of states compares well to the one obtained by inelastic neutron scattering. The stretching frequency of the hydrogen bridge is different from the stretching, bending and wagging frequencies of the SiH and SiH_2 groups, thus should be visible by IR spectroscopic techniques.

[1] A. V. Shah, R. Platz, and H. Keppner, Sol. Energy Mater. Sol. Cells **38**, 501 (1995).

[2] E. A. G. Hamers, M. N. van den Donker, B. Stannowski, R. Schatmann, and G. J. Jongerden, Plasma Process. Polym. **4**, 275 (2007).

[3] D. C. Allan, J. D. Joannopoulos, and W. B. Pollard, Phys. Rev. B **25**, 1065 (1982).

[4] R. Car and M. Parrinello, Phys. Rev. Lett. **60**, 204 (1988).

[5] F. Buda, G. L. Chiarotti, R. Car, and M. Parrinello, Phys. Rev. B **44**, 5908 (1991).

[6] P. A. Fedders and D. A. Drabold, Phys. Rev. B **47**, 13277 (1993).

[7] B. Tuttle and J. B. Adams, Phys. Rev. B **53**, 16265 (1996).

[8] G. R. Gupte, R. Prasad, V. Kumar, and G. L. Chiarotti, Bull. Mater. Sci. **20**, 429 (1997).

[9] M. Tosolini, L. Colombo, and M. Peressi, Phys. Rev. B **69**, 075301 (2004).

[10] P. Klein, H. M. Urbassek, and T. Frauenheim, Phys. Rev. B **60**, 5478 (1999).

[11] A. A. Valladares, F. Alvarez, Z. Liu, J. Sticht, and J. Harris, Eur. Phys. J. B **22**, 443 (2001).

[12] R. A. Street, *Hydrogenated Amorphous Silicon* (Cambridge University Press, Cambridge, 1991).

[13] J. P. Perdew, J. A. Chevary, S. H. Vosko, K. A. Jackson, M. R. Pederson, D. J. Singh, and C. Fiolhais, Phys. Rev. B **46**, 6671 (1992).

[14] G. Kresse and J. Hafner, Phys. Rev. B **47**, 558 (1993).

[15] G. Kresse and J. Furthmüller, Phys. Rev. B **54**, 11169 (1996).

[16] G. Kresse and D. Joubert, Phys. Rev. B **59**, 1758 (1999).

[17] P. E. Blöchl, Phys. Rev. B **50**, 17953 (1994).

[18] M. Methfessel and A. T. Paxton, Phys. Rev. B **40**, 3616 (1989).

[19] H. J. Monkhorst and J. D. Pack, Phys. Rev. B **13**, 5188 (1976).

[20] G. Lucovsky, R. J. Nemanich, and J. C. Knights, Phys. Rev. B **19**, 2064 (1979).

[21] R. E. I. Schropp and M. Zeman, *Amorphous and Microcrystalline Silicon Solar Cells: Modeling, Materials and Device Technology* (Kluwer Academic Publishers, Norwell, 1998).

[22] I. Štich, R. Car, and M. Parrinello, Phys. Rev. B **44**, 11092 (1991).

[23] K. Laaziri, S. Kycia, S. Roorda, M. Chicoine, J. L. Robertson, J. Wang, and S. C. Moss, Phys. Rev. B **60**, 13520 (1999).

[24] A. Filipponi, F. Evangelisti, M. Benfatto, S. Mobilio, and C. R. Natoli, Phys. Rev. B **40**, 9636 (1989).

[25] S. Vignoli, P. Mélinon, B. Masenelli, P. R. i Cabarrocas, A. M. Flank, and C. Longeaud, J. Phys.: Condens. Matter **17**, 1279 (2005).

[26] M. Wakagi, K. Ogata, and A. Nakano, Phys. Rev. B **50**, 10666 (1994).

[27] W. Schülke, Philos. Mag. B **43**, 451 (1981).

[28] R. Bellisent, A. Menelle, W. S. Howells, A. C. Wright, T. M. Brunier, R. N. Sinclair, and F. Jansen, Physica B **156-157**, 217 (1989).

[29] N. W. Ashcroft and D. C. Langreth, Phys. Rev. **156**, 685 (1967).

[30] The fact that the experimental static structure factors are measured over a finite interval in reciprocal space, results in unphysical negative values of the radial distribution function at small distances.

[31] J. Fortner and J. S. Lannin, Phys. Rev. B **39**, 5527 (1989).

[32] S. Kugler, L. Pusztai, L. Rosta, P. Chieux, and R. Bellissent, Phys. Rev. B **48**, 7685 (1993).

[33] L. Giacomazzi, P. Umari, and A. Pasquarello, Phys. Rev. B **74**, 155208 (2006).

[34] G. Kresse, J. Furthmuller, and J. Hafner, Europhys. Lett. **32**, 729 (1995).

[35] The quantum effects would be bigger at low temperature. Feldman *et al.* obtained a significant broadening, for pure amorphous silicon at 10K, originating from quantum-mechanical nature of the nuclei. J. L. Feldman, N. Bernstein, D. A. Papaconstantopoulos, and M. J. Mehl, J. Phys.: Condens. Matter **16**, S5165 (2004).

[36] S. Kugler, G. Molnar, G. Peto, E. Zsoldos, L. Rosta, A. Menelle, and R. Bellissent, Phys. Rev. B **40**, 8030 (1989).

[37] G. D. Cody, T. Tiedje, B. Abeles, B. Brooks, and Y. Goldstein, Phys. Rev. Lett. **47**, 1480 (1981).

[38] C. Kittel, *Introduction to Solid State Physics*, 7th ed. (Wiley, New York, Chichester, 1996).

[39] G. Kresse and J. Hafner, Phys. Rev. B **55**, 7539 (1997).

[40] P. Anderson, Phys. Rev. Lett. **34**, 953 (1975).

[41] D. A. Drabold, P. A. Fedders, S. Klemm, and O. F. Sankey, Phys. Rev. Lett. **67**, 2179 (1991).

[42] The distinction between a defect state and a band tail state is based on the degree of localization. We define a threshold value of 0.1, since a vast majority of the wave functions that contribute to a defect state have smaller participation ratios.

[43] M. Fornari, M. Peressi, S. Gironcoli, and A. Baldereschi, Europhys. Lett. **47**, 481 (1999).

[44] R. Fisch and D. C. Licciardello, Phys. Rev. Lett. **41**, 889 (1978).

[45] R. N. Sinclair, A. C. Wright, T. M. Brunier, A. C. Hannon, S. M. Bennington, and F. Jansen, J. Non-Cryst. Solids **192-193**, 243 (1995).

[46] D. A. Drabold, P. A. Fedders, O. F. Sankey, and J. D. Dow, Phys. Rev. B **42**, 5135 (1990).

[47] P. A. Fedders, D. A. Drabold, and S. Klemm, Phys. Rev. B **45**, 4048 (1992).

[48] E. Kim and Y. H. Lee, Phys. Rev. B **49**, 1743 (1994).

[49] P. Klein, H. M. Urbassek, and T. Frauenheim, Comput. Mater. Sci. **13**, 252 (1999).

[50] A. Valladares, R. M. Valladares, F. Alvarez-Ramirez, and A. A. Valladares, J. Non-Cryst. Solids **352**, 1032 (2006).